Structural basis for promiscuous action of monoterpenes on TRP channels

Nguyen, Thi Hong Dung

Doctor of Phylosophy

Department of Physiological Sciences,

School of Life Science,

The Graduate University for Advanced Studies,

SOKENDAI

2020

Index

1. Abstract

Monoterpenes are major constituents of plant-derived essential oils and have long been widely used for therapeutic and cosmetic applications. The monoterpenes menthol and camphor are agonists or antagonists for several TRP channels such as TRPM8, TRPV1, TRPV3 and TRPA1. However, which regions within TRPV1 and TRPV3 confer sensitivity to monoterpenes or other synthesized chemicals such as 2-APB are unclear. In this study I identified conserved arginine and glycine residues in the linker between S4 and S5 that are related to the action of these chemicals and validated these findings in molecular dynamics simulations. The involvement of these amino acids differed between TRPV3 and TRPV1 for chemical-induced and heat-evoked activation. These findings provide the basis for characterization of physiological function such as thermal sensation, nociception and disease. In addition, the structural basis for promiscuous action of monoterpenes on TRPV3 and TRPV1 in this study will provide the better understanding about biophysical properties of ion channels to target for drug design.

2. Introduction

Organisms use sensors such as transient receptor potential (TRP) ion channels to adapt to environmental changes. Members of the TRP ion channel family play important roles as polymodal sensors to detect and respond to changes in temperature, pH, voltage, osmolarity, and exogenous molecules involved in taste, smell, and pheromone responses[1]. Channels in this family include TRP vanilloid 1 (TRPV1), TRP vanilloid 3 (TRPV3) and TRP melastatin 8 (TRPM8) that are all crucial for sensing temperature and natural compounds[2,3]. TRPV1 is physiologically important for thermal and chemical nociception in sensory neurons and is activated by capsaicin, toxins, pH, and temperature in the noxious range (>42 °C). The third member of the TRPV subfamily, TRPV3, is also a heat sensor. TRPV3 is expressed in various tissues and organs, but the most intensive expression is in skin epithelial cells. TRPV3 is believed to be responsible for sensation of warm temperature ranging from 35-39 °C[4], but has also been reported to be initially activated by noxious heat (>50 °C) and sensitized to activation in response to warm temperature[5]. Chemical agonists of TRPV3 include spice extracts that contain monoterpenes such as menthol, camphor and carvacrol, synthetic agents (including 2-aminoethoxy diphenylborate, 2-APB) and unsaturated fatty acids[6]. Whereas many TRPV subfamily members act as heat sensors, the TRPM8 channel is known to be involved in sensations induced by cool temperatures (<22 °C) and menthol[3,7]. TRMP8 is highly expressed in sensory neurons of trigeminal and dorsal root ganglia as well as in the prostate epithelium[8]. PIP_2 regulates TRM8 activity and PIP_2 depletion can desensitize the channel.

The six TRP subfamilies (TRPC, TRPV, TRPM, TRPA, TRPP, and TRPML) all have a tetrameric assembly consisting of putative six transmembrane secondary structures (S1-S6) with intracellular N and C termini. Each subunit has a re-entrant loop with a pore loop (P) comprising 1-2 small pore helices (H1/H2) that is located between S5 and S6 (S5-P-S6). The S1-S4 and S5-P-S6 are connected by the S4-S5 linker. The structures of several TRP channels

were recently extensively clarified by cryo-EM single-particle analysis[9-12]. The combination of cryo-EM microscopy with nanodisc technology allowed the efficient determination of the location of annular and regulatory lipids[10,13,14,15]. Lipids in cellular membranes are important regulators that can functionally modulate many TRP channels by direct or specific interactions, especially in the case of phosphatidylinositides (PIP_2) and cholesterol. Gao et al. reported in 2016 that a binding pocket in the S4-S5 linker region for vanilloid ligands is shared with that for PIP_2. Tightly bound PIP_2 works as a co-factor that stabilizes TRPV1 in its resting state by serving as a competitive vanilloid antagonist and a negative allosteric modulator[9,10]. In a recent study, Singh et al. observed two non-protein densities, presumably representing lipids, in each subunit of the TRPV3 tetramer. The pockets for lipids are located in the intracellular half of S1-S4 domains and C-terminus of the TRP domain, which are analogous to the pocket for putative lipids in other TRPV channels[11]. Lipid location and function were also clarified in recent studies of the TRPM8 structure[13,14]. Yin et al. reported in 2019 that for TRPM8 PIP_2 can effectively control conformational transitions associated with gating and enhance the potency of agonist binding[12,13].

Menthol, a natural non-reactive cooling compound that has three asymmetric carbon atoms and a molecular formula of $C_{10}H_{20}O$, is widely used in oral hygiene products, cosmetics, pesticides and pharmaceuticals, and is also used as a flavoring agent in foods. The major form of menthol found in nature is (−)-menthol (*l*-menthol), which is frequently studied since it has better cooling properties than other isomers[16,17]. Menthol is a well-known TRPM8 activator, and is required for cool thermosensation *in vivo*[3,7]. Menthol can also activate TRPV3 and has bimodal effects on mouse TRPA1[18,19]. Moreover, several amino acids were shown to be involved in the binding site of menthol in mouse TRPM8 (Y745 in S1, R842 in S4 and Y1005 in TRP domain)[20,21] and human TRPA1 (S873 and T874 in S5)[22]. Furthermore, it was previously reported that menthol inhibits capsaicin-activated human TRPV1 activity[23],

indicating that it shows promiscuous actions toward several TRP channels. However, no consensus has been reached regarding menthol binding sites, especially for TRPV3.

Other structurally-related monoterpenes such as camphor, carvacrol and 1,8-cineol can also regulate several TRP channels in different ways. For example, camphor activates mammalian TRPV1 and TRPV3, but inhibits rat TRPA1[20]. Interestingly, some studies indicated that these natural compounds can insert into biological membranes where they can cause significant alterations in numerous physico-chemical characteristics of lipid bilayers[24-27]. A central question arises about whether the effects of these small and hydrophobic compounds are mediated directly, via direct interaction with ion channels integrated in the membrane, and/or indirectly through alterations in the physico-chemical characteristics of lipid membranes that have indirect effects on channel function.

I have characterized the pharmacological effects of menthol and other structurally- related monoterpenes on several TRP channels including TRPV1, TRPV3 and TRPM8. I show for the first time an agonistic effect of menthol on TRPV1. I also identified two amino acids in the S4-S5 linker that are involved in the agonistic effect of menthol on TRPV1 (R557K and G563S) and TRPV3 (R567K and G573S).

3. Materials and Methods

Construction of mutant mouse TRPV1, TRPV3 or TRPM8

TRPV3 or TRPM8 point mutants were constructed using a PrimeSTAR mutagenesis Basal kit according to the manufacturer's recommendations (Takara Bio Inc., Shiga, Japan). TRPV1 point mutants were constructed using PrimeSTAR GXL DNA polymerase (Takara Bio Inc., Shiga, Japan). Point mutations were introduced by PCR using mouse TRPV1–pcDNA3, TRPV3–pcDNA3, and TRPM8–pcDNA5/FRT as templates with oligonucleotide primers (Table 1) containing the intended mutations. The amplified PCR products consisting of PcDNA3 vectors containing rat TRPV1 or mouse TRPV3 and pcDNA5/FRT vectors containing mouse TRPM8 that were transformed into *Escherichia coli* and then purified using standard procedures. The entire TRPV1, TRPV3, and TRPM8 coding sequences were determined to confirm that only the intended mutations were introduced.

Cell culture

Human embryonic kidney-derived 293T (HEK 293T) cells were maintained at 37 °C and 5% CO_2 in Dulbecco's modified Eagle's Medium (WAKO Pure Chemical Industries, Osaka, Japan) containing 10% fetal bovine serum (Biowest SAS, Nuaillé, France), 100 units ml^{-1} penicillin (Invitrogen Corp.), 100 μg ml^{-1} streptomycin (Invitrogen Corp.), and 2 mm GlutaMAX (Invitrogen Corp.). For patch-clamp recordings, 1 μg mouse TRPM8 in pcDNA5/FRT, mouse TRPV1 or mouse TRPV3 in pcDNA3 vector and 0.1 μg pGreen Lantern 1 cDNA were transfected to HEK293T cells cultured in 35 mm dishes using Lipofectamine Plus Reagent (Invitrogen Corp.). After incubating for 3-4 h, the cells were reseeded on coverslips and further incubated at 33 °C for mouse TRPV3 or 37 °C for mouse TRPV1 or mouse TRPM8 in 5% CO_2. Patch-clamp recordings were performed 1 day after transfection.

Chemicals

l-menthol, capsaicin, and 2-aminoethoxydiphenyl borate were purchased from Sigma-Aldrich (St. Louis, MO, USE) and camphor was purchased from WAKO chemicals (Tokyo, Japan). 2-APB was dissolved in DMSO for stock solutions (1 M) and camphor or *l*-menthol was dissolved in ethanol as a stock solution (3 M) and diluted to the final concentration using bath solution.

Electrophysiology

For whole-cell experiments, the experimental solutions were: bath solution: 140 mM NaCl, 5 mM KCl, 2 mM $MgCl_2$, 5mM EGTA, 10 mM HEPES and 10 mM glucose at pH 7.4 adjusted with NaOH; pipette solution: 140 mM CsCl, 5 mM EGTA; and 10 mM HEPES at pH 7.4 adjusted with CsOH. Data from whole-cell voltage-clamp recordings were acquired at 10 kHz throughout the experiments and filtered at 5 kHz for analysis (Axon 200B amplifier with pCLAMP software, Axon Instruments, Foster City, CA, USA). The membrane potential was clamped at −60 mV. Pipette resistance and series resistance were compensated.

All experiments were performed at 25 °C unless otherwise stated. Heat stimulation was induced by increasing the bath temperature using a pre-heated solution warmed in an inline heater (1 °C s^{-1}, with a maximum of 55 °C). The temperature was monitored using a thermocouple (TC-344; Warner Instruments, Hamden, CT, USA) placed within 100 μm of the patch-clamped cell. The heat stimulation was stopped upon confirming that TRPV3 currents were desensitized or inactivated. Temperature profiles and Arrhenius plots for the data from whole-cell voltage-clamp recordings were calculated using Origin 8.5 software (OriginLab, Northampton, MA, USA). The absolute current values were plotted on a log scale against the reciprocal of the absolute temperature (*T*) (Arrhenius plot), and the temperature threshold for channel activation was determined by the temperature that caused a change in the slope. For

current density analysis of TRPV3 channels, the peak currents induced by heat or chemical stimulation were measured and presented as pA pF^{-1}.

Molecular dynamics simulation

To confirm stable binding of monoterpenes, molecular dynamics (MD) simulations of TRPV3 was performed with a *l*-menthol molecule or a camphor molecule. The PDB structure (ID: 6DVW) was employed for the initial structure of TRPV3[11]. Because the N-terminal (residues 1-114) and C-terminal (residues 759-791) residues are missing in the PDB structure, the N-terminus (residue 115) and C-terminus (residue 758) were blocked by the acetyl group and the N-methyl group, respectively. Docking conformations of the *l*-menthol and camphor molecules with TRPV3 were obtained by using the docking program AutoDock[28] . The N- and C-terminal residues (up to residue 391 and after residue 720) were removed in the MD simulations. MD simulations for a R567F mutant of TRPV3 with *l*-menthol or camphor was also performed. The initial conformation of the R567F mutant was prepared by replacing the arginine residue (R567) with a phenylalanine residue.

The electrostatic charges of the atoms of *l*-menthol and camphor molecules were determined by the restrained electrostatic potential (RESP) fits[29]. Quantum chemical calculations were performed using the Gaussian16 program[30]. Structure optimization and electrostatic potential calculations were carried out using the Hartree-Fock level with a 6-31G(d) basis set. As for parameters other than the atomic electrostatic charges, general Amber force field parameters[31] were employed for these molecules.

The MD simulations were performed using the Generalized-Ensemble Molecular Biophysics (GEMB) program developed by Dr. Hisashi Okumura (Exploratory Research Center on Life and Living Systems, Okazaki, Japan). This program has been used for several proteins and peptides[32,33]. The AMBER parm14SB force field[34] was used for TRPV3. The

cubic unit cell with a side length of 200 Å with the periodic boundary conditions was used. The electrostatic potential was calculated by the particle-mesh Ewald method[35]. The cut-off distance for the Lennard-Jones potential was 12 Å. The Nosé-Hoover thermostat[36,37] was used to control the temperature at 310 K. The multiple-time-step method[38] was used. The time step was taken to be Δt=0.5 fs for the bonding interactions and Δt=2.0 fs for the non-bonding interactions. To maintain the atomic structure of the TRPV3 in a vacuum, N, C_α, and C atoms of the residues that form α-helix structures were restrained with a harmonic potential, as in ref.[39]. Each MD simulation was performed for 100 ns.

Statistical analysis

Data in all figures are shown as means ± standard error of the mean (S.E.M.). Statistical analysis was performed by Student's *t* test or analysis of variance (1-way ANOVA) with Bonferroni correction using Origin 8.5 software. Probability values (*P*) of <0.05 were considered statistically significant. EC_{50} was determined using Origin 8.5 software.

4. Results

Confirmation of mutations that specifically affect menthol responses in TRPM8

I made histidine substitutions at Y745 in the S1 transmembrane segment and R842 in the S4 transmembrane segment of mouse TRPM8 (mTRPM8; Figs. 1 and 2A); these amino acids are putative binding sites for menthol on TRPM8[21,40]. I then used a whole-cell patch-clamp method to test the agonistic effects of menthol (Fig. 2B) on these mutants expressed in transiently transfected HEK293T cells. Consistent with previous reports, menthol (500 μM)-evoked currents for mTRPM8 Y745H and R842H mutants were much smaller than those of wild type (WT) mTRPM8 (Fig. 2C, D), while their cold sensitivity was preserved.

Involvement of S4–S5 region residues R567 and G573 in agonist responses by mTRPV3

I hypothesized that amino acids associated with the effects of menthol on TRPV3 and TRPM8 would be similar and found three candidate residues, tyrosine (Y) in S1 and arginine (R) and glycine (G) in the S4-S5 linker (Figs. 1 and 3A). I first found that Y448 in mTRPV3 is not involved in menthol-evoked mTRPV3 activation (Fig. 3B), which is a little bit inconsistent with the report that TRPV3 channel activity is potentiated by PIP_2 hydrolysis[41], while PIP_2 regulates TRPM8 activity through binding to S1, probably along with menthol[13]. Camphor and 2-APB sensitivities were not changed for mTRPV3-Y448H (Fig. 3C, D). However, unlike WT mTRPV3, menthol did not activate mTRPV3-G573S, whereas heat-evoked activation was still observed (Fig. 4A, B), indicating that G573 is involved in menthol-evoked activation of mTRPV3. This mutant also lost sensitivity to camphor and 2-APB, but was activated by heat (Fig. 4C-H), which is consistent with a previous report[42].

Next, I examined the possible involvement of R567 in menthol-evoked activation of TRPV3. Menthol-activated currents were very small in mTRPV3-R567K, whereas those evoked by camphor were similar between WT and mTRPV3-R567K (Fig. 5A-C), which is in contrast to

the phenotype seen for mTRPV3-G573S. The results were the same when the application sequence was changed (Fig. 6A, B). The 2-APB sensitivity was also similar between WT and mTRPV3-R567K (Fig. 6C, D). These data indicated that G573 and R567 are differently involved in the chemical responses of mTRPV3 wherein G573 is involved in responses to menthol, camphor, and 2-APB, while R567 is involved in menthol action, but not in camphor and 2-APB sensitivity.

Involvement of S4/S4–S5 region residues R557 and G563 in the agonistic effect of menthol on TRPV1

Naturally-occurring TRP ligands show some degree of promiscuity as shown above. Notably, menthol is not only a TRPM8 agonist, but can also activate mammalian TRPV3[19,40] and TRPA1[18], suggesting that the mechanism associated with the response to menthol is conserved across several TRP channels. Indeed, it was previously reported that hTRPV1 currents activated by capsaicin were dose-dependently inhibited by menthol with IC_{50} values of 1.2 ± 0.2 mM[23], whereas mTRPM8 activation by menthol has EC_{50} values that range from 4 to 80 μM[3,4]. Therefore, I first attempted to examine the agonistic effect of high concentrations of menthol on TRPV1 since both the tyrosine in S1 and arginine and glycine in the S4/S4-S5 linker of rTRPV1 are conserved (Fig. 7A). I did not examine Y441 since capsaicin sensitivity was altered in rTRPV1-Y441H (Fig. 7B) and rTRPV1-Y441H lost heat sensitivity (data not shown). The importance of this aromatic cluster is underscored by previous studies demonstrating that replacement of Y441 by small non-aromatic residues resulted in non-functional channels[43,44].

On the other hand, I unexpectedly observed rTRPV1 activation by 3 mM menthol (Fig 7C), although I could not determine EC_{50} values of menthol-evoked activation for rTRPV1 since solutions having high concentrations of menthol could not be prepared. As expected, rTRPV1-

G563S and rTRPV1-R557K lost menthol-evoked activation, although capsaicin (1μM) sensitivity was not affected (Fig 7C-E, Fig. 8). I next examined the effects of camphor and 2-APB since their effects on mTRPV3 differed between G573 and R567 (Figs. 3 and 5). Interestingly, neither camphor nor 2-APB could activate rTRPV1-G563S or rTRPV1-R557K (Fig. 9).

Importance of positive charge at R567 for activation of mTRPV3 by camphor

The above data indicated that the involvement of glycine and arginine in monoterpene-evoked activation differs between mTRPV3 and rTRPV1. Due to the structural similarity of menthol and camphor as monoterpenes, we explored whether the charge at R567 is important for the action of camphor by comparing the response of WT, R567K, R567H, R567A, and R567F to camphor treatment. I first confirmed that R567F was not sensitive to menthol (Fig. 10). Moreover, since the response to 2-APB was not affected for the R567 mutants, I compared the ratio of camphor-activated currents to 2-APB-activated currents. Camphor-evoked mTRPV3 activation was markedly reduced for R567A and R567F compared with WT, R567K and R567H (Fig. 10). These data confirm the importance of R567, and particularly the positive charge of R, for activation of mTRPV3. I thus conclude that both arginine and glycine are involved in monoterpene-evoked activation of mTRPV3 and rTRPV1.

Importance of the S4-S5 linker region for heat-evoked activation of TRPV1, but not TRPV3

Notably, temperature sensitivity is a hallmark of TRPV1 and TRPV3 channel function[4,45,46]. Mutagenesis or deletion studies indicated several regions that are important for heat-induced activation of heat-activated TRP channels. The heat-sensitive regions of TRPV channels are located at the N-terminal ankyrin repeat domains in TRPA1[47], a membrane-proximal N-

terminal segment in TRPV1, TRPV2, and TRPV3[5,48], the C terminus of TRPV1[49-51], and the pore domain of TRPV1 and TRPV3[52-55]. Residues that could be involved in temperature sensing may be scattered throughout the receptors rather than forming a defined temperature-sensing domain[56]. I thus considered whether glycine and arginine, which are involved in monoterpene-evoked activation, are also involved in heat-evoked activation. I first examined temperature-evoked activation of mTRPV3-G573S and mTRPV3-R567K in HEK293T cells by increasing the temperature of the bath solution from 25 °C to 50 - 53 °C. Similar to WT mTRPV3, large inward currents were observed for both mTRPV3-G573S and mTRPV3-R567K and no change in temperature threshold was observed (Fig. 11A-C). On the other hand, rTRPV1-G563S and rTRPV1-R557K did not exhibit heat-evoked activation (Fig. 11D, E), and capsaicin-sensitivity was also not affected (Figs. 7E and 8). These data indicated that glycine and arginine in S4-S5 of mTRPV3 and rTRPV1 have a different involvement in heat-evoked activation and that G563 and R557 are involved in heat-evoked activation of rTRPV1, as was previously reported[44].

Stable binding of menthol and camphor to mouse TRPV3

Typical snapshots obtained from the MD simulations are shown in Fig. 12A-12D. The oxygen atom of menthol and camphor forms hydrogen bonds with amino groups ($-NH_2$) of R567, as shown in Fig. 12A and 12B. Because of these hydrogen bonds, menthol and camphor bind stably to R567 in mouse TRPV3. On the other hand, in the R567F mutant, such hydrogen bond is not formed because phenylalanine does not have an amino group. Thus, menthol and camphor are not fixed in the R567F mutant and sometimes away from F567. To observe these phenomena more clearly, the time series of the distances between menthol/camphor and R567/F567 were calculated, as shown in Fig. 12E and 12F. Here, this distance was calculated as the shortest distance between the heavy atoms (except hydrogen) of menthol/camphor and

those of R567/F567. This distance fluctuated a little around 3 Å in the wild type TRPV3, whereas it fluctuated in the wider range from 3 to 9 Å in the R567F mutant. These results show that both menthol and camphor bind to R567 firmly by the hydrogen bond in the wild type, but they are not fixed and fluctuate in the R567F mutant.

5. Discussion

To date, little is known about how different monoterpene compounds are sensed by TRPV3 and the sites at which they act are also unclear. Investigation of the actions of monoterpene agonists on TRPV3 will provide clues to clarify the structural basis of activation, which could lead to increased understanding of the role of TRPV3 in physiological function and in disease. I can also exploit the promiscuous actions of monoterpenes toward several TRP channels as an important research tool to characterize the physiological function and biophysical properties of ion channels. Several monoterpene compounds such as menthol and camphor, and the synthetic small, hydrophobic compound 2-APB all activate TRPV1 and TRPV3, even though these two channels share only about 39% amino acid sequence identity[20,57,58]. In the present work, I identified the putative shared amino acids that are involved in menthol, camphor, and 2-APB-evoked activation in TRPV3 and TRPV1 and these residues were further confirmed in MD simulations. These results showed that the conserved glycine and arginine residues in the S4-S5 linker of TRPV3 (G573, R567) and TRPV1 (G563, R557) are required for menthol- and camphor-evoked activation.

As previously reported, several amino acids function as binding sites for menthol in mouse TRPM8 (Y745 (S1), R842 (S4), and Y1005 (TRP domain))[21,40]. Among these, Y745 and R842 are conserved in TRPV1 and TRPV3. Y745, R842, and Y1005 are proximal in the TRPM8 structure, but do not lie close to one another in the TRPV1 and TRPV3 structures (Fig. 1). PIP_2, a positive modulator of the TRPM8 channel, but not of TRPV1, can bind to the pocket formed by the pre-S1 elbow, S1 of one subunit and S5 in the neighboring subunit[13]. On the other hand, Karashima et al. showed that menthol has a bimodal action on mTRPA1 via a mechanism that involves S876 and T877 in S4-S5 linker/S5 region[3]. These results suggest that the binding pocket and mechanistic action of menthol toward TRPM8 would be distinguishable from that for other TRP channels, and that the S4-S5 linker/S5 region is critical for the action of menthol

in TRPV1, TRPV3 and TRPA1, but not TRPM8.

In this study I revealed for the first time the activation of rat TRPV1 by menthol, which had characteristics similar to that seen for camphor-mediated activation of rat TRPV1. Xu et al. showed that camphor has strong desensitizing activity rat TRPV1, and suggested that the combination of desensitization of rat TRPV1 and inhibition of rat TRPA1 could provide a new explanation for the pain-relieving properties of menthol[20]. These actions could be parallel to the analgesic property of menthol, since high concentrations of menthol inhibit both mammalian TRPA1 and TRPV1[19,23].

In my study I found some differences in menthol, camphor, and 2-APB binding sites between TRPV1 and TRPV3. The single point mutations G563S and R557K in rat TRPV1 eliminated sensitivity to menthol, camphor, and 2-APB (Figs. 7 and 9), whereas the G573S and R567K mutations exhibited different responses from those seen for mouse TRPV3. G573S lost sensitivity to all three compounds, and the sensitivity of R567K to menthol was affected, but that for 2-APB was not. The structural reconstructions by Zubcevic et al. did not enable unambiguous identification of 2-APB in human TRPV3, but they did observe that one of the distinct non-protein densities is located in the S4-S5 interface pocket when 2-APB is present, suggesting that 2-APB binds this pocket[59], which is consistent with my results. Although the structures of camphor and menthol are similar, the positive charge at R567 was necessary for activation of mouse TRPV3 by camphor (Fig. 10). These results could be explained in part by the smaller size of camphor relative to menthol that requires the positive charge to promote an effective fit in the binding pocket formed by G573 and R567.

Remarkably, the G573S mutation of human TRPV3 corresponding to mouse TRPV3-G573S in my study is associated with Olmsted syndrome, which is characterized by bilateral mutilating palmoplantar keratoderma and periodic keratotic plaques accompanied by severe itching[60,61]. This mutation in mouse TRPV3 was reported to show large basal currents in the

absence of agonists and no responses to 2-APB and camphor in either HEK293 cells or *Xenopus* oocytes[42,62]. Meanwhile, in this study basal currents before stimulation were not larger than those seen for WT-expressing HEK293T cells. I also did not see 2-APB and camphor sensitivity for this mutant (Fig. 4) or differences in heat-sensitivity between mouse TRPV3-WT and G573S (Fig. 11). The reason for the apparent difference in the basal channel activities seen in this study relative to those seen in previous studies is unclear. However, the cryo-EM-based structure indicates that G573 in the S4−S5 linker lies at the junction with the lower part of S4, S5, the TRP domain, and the lower part of S6[59]. This structural feature raises the possibility that mouse TRPV3-G573 is involved in channel gating in concert with W692, which is in the vicinity of G573 and is reported to cause large basal currents[42,62]. However, the mechanisms responsible for this high basal activity remain unknown.

The mutants G563S and R557K affected the heat sensitivity of rat TRPV1, while G573S and R567K exhibited similar heat-evoked responses in WT mouse TPRV3, indicating that the involvement of these two corresponding residues in heat sensitivity differs between mouse TRPV3 and rat TRPV1 (Fig. 11). Results in the TRPV3 mutants seem to align with the recent cryo-EM structure of TRPV3 where it is shown that temperature-mediated opening of TRPV3 is induced from the conformational changes in the extracellular part of the pore domain and then leads to the channel opening[59]. No clear evidence for the mechanisms of heat-evoked activation of TRP channels is available, although multiple studies involving mutant analyses or cryo-EM studies showed that several regions are involved in the heat-sensitivity of TRPV1 and TRPV3[49-52,63,64]. My results indicate that the activation mechanisms of heat and chemical stimulation of TRPV3 differ, but could have somehow converged in the sensitivity of TRPV1 to some chemicals such as monoterpenes, suggesting that mechanisms for heat sensitivity of TRPV3 and TRPV1 are different. These results could clarify the mechanisms of heat-evoked activation of thermosensitive TRP channels.

Results of the MD simulation data indicated tight binding of menthol and camphor to the pocket formed by arginine and glycine in the S4-S5 linker of mouse TRPV3 (Fig. 12). However, whether these compounds directly induce activation upon binding to channels is unclear. Menthol and camphor, as mentioned earlier, are small and hydrophobic (Log p-value of 3.4 and 2.74[25,65], respectively). Several previous studies showed that the physico-chemical characteristics of lipid bilayer membranes such as membrane fluidity and thickness can be modified by menthol and other related monoterpenes[24,25,27,66]. Interestingly, beyond the positive effects of PIP_2 in menthol-evoked activation of TRPM8, previous studies also reported the location of putative lipids in several regions including the S4-S5 linker in TRPV1, TRPV3, and TRPV6[10,11,59]. For example, the pocket at the S4-S5 interface that binds to an activating lipid in TRPV6 (the density observed in this pocket may represent the natural lipid agonist in TRPV6 binding sites), and the exchange between phosphoinositides and activator/inhibitor in this vanilloid-binding pocket could allosterically regulate TRPV1. Indeed, 2-APB is proposed to induce TRPV3 activation and inhibit TRPV6 by modulating interactions with bound lipids[11,67]. Thus, I suggest that monoterpenes could modulate the activity of several TRP channels including TRPM8, TRPV1, and TRPV3 by manipulating interactions with bound lipids, particularly since monoterpenes can act on several channels and the binding pocket locations overlapped with those for lipids. Activation or inhibition of TRP channel activity by monoterpenes and the intensity with which these agents act could depend on the regulatory roles of lipids for TRP channel gating and on what kinds of lipid, such as PIP_2 and cholesterol, bind to the channels. However, I cannot rule out that both changes in the physico-chemical properties of the lipid bilayer and direct binding of hydrophobic compounds to ion channels explain the actions of menthol and other monoterpenes on the functional properties of TRP channels and other ion channels.

6. Acknowledgements

I would like to thank all the people who contributed in some way to the work described in this thesis. I would like to express my sincere gratitude to Prof. Makoto Tominaga for his patience, and excellent supporting from the first day I joined his lab until present. Without his empathy and persistent guidance, this dissertation would not have been possible.

I would also like to show gratitude to Associate Professor Hisashi Okumura and Assistant Professor Satory G. Itoh for their performing the MD simulations. I would like to thank Mrs. Fukuta Naomi for her dedicating teaching for my experiments related to Molecular work. Especially, I really appreciate the kind and cozy supporting from Mrs. Yoshimi Ito and Ms. Jing Lei who helped me to overcome the difficult circumstances of my life in Japan.

During times I study in here, I really appreciate every member who always help me in daily life and research activities. I sincerely appreciate my husband and my family for their encouragement and their supporting. Many thanks to my son because his appearance make me stronger and have more motivation to complete all of the works.

The author also thanks. In addition, the author thanks every member of Professor Tominaga's laboratory for their supports.

7. References

1 Clapham, D. E. in *Nature* Vol. 426 517-524 (2003).

2 Caterina, M. J. *et al.* The capsaicin receptor: A heat-activated ion channel in the pain pathway. *Nature* **389**, 816-824, doi:10.1038/39807 (1997).

3 McKemy, D. D., Neuhausser, W. M. & Julius, D. Identification of a cold receptor reveals a general role for TRP channels in thermosensation. *Nature* **416**, 52-58, doi:10.1038/nature719 (2002).

4 Peier, A. M. *et al.* A heat-sensitive TRP channel expressed in keratinocytes. *Science* **296**, 2046-2049, doi:10.1126/science.1073140 (2002).

5 Liu, B. & Qin, F. Single-residue molecular switch for high-temperature dependence of vanilloid receptor TRPV3. *Proceedings of the National Academy of Sciences of the United States of America* **114**, 1589-1594, doi:10.1073/pnas.1615304114 (2017).

6 Hu, H. Z. *et al.* Potentiation of TRPV3 channel function by unsaturated fatty acids. *Journal of Cellular Physiology* **208**, 201-212, doi:10.1002/jcp.20648 (2006).

7 Peier, A. M. *et al.* A TRP channel that senses cold stimuli and menthol. *Cell* **108**, 705-715, doi:10.1016/S0092-8674(02)00652-9 (2002).

8 Brauchi, S., Orio, P. & Latorre, R. Clues to understanding cold sensation: Thermodynamics and electrophysiological analysis of the cold receptor TRPM8. *Proceedings of the National Academy of Sciences of the United States of America* **101**, 15494-15499, doi:10.1073/pnas.0406773101 (2004).

9 Cao, E., Liao, M., Cheng, Y. & Julius, D. TRPV1 structures in distinct conformations reveal activation mechanisms. *Nature* **504**, 113-118, doi:10.1038/nature12823 (2013).

10 Gao, Y., Cao, E., Julius, D. & Cheng, Y. TRPV1 structures in nanodiscs reveal mechanisms of ligand and lipid action. *Nature* **534**, 347-351, doi:10.1038/nature17964 (2016).

11 Singh, A. K., McGoldrick, L. L. & Sobolevsky, A. I. Structure and gating mechanism of the transient receptor potential channel TRPV3. *Nature Structural and Molecular Biology* **25**, 805-813, doi:10.1038/s41594-018-0108-7 (2018).

12 Yin, Y. *et al.* Structure of the cold- And menthol-sensing ion channel TRPM8. *Science* **359**, 237-241, doi:10.1126/science.aan4325 (2018).

13 Yin, Y. *et al.* Structural basis of cooling agent and lipid sensing by the cold-activated TRPM8 channel. *Science* **363**, doi:10.1126/science.aav9334 (2019).

14 Diver, M. M., Cheng, Y. & Julius, D. Structural insights into TRPM8 inhibition and desensitization. *Science* **365**, 1434-1440, doi:10.1126/science.aax6672 (2019).

15 Shimada, H. *et al.* The structure of lipid nanodisc-reconstituted TRPV3 reveals the gating mechanism. *Nat Struct Mol Biol*, doi:10.1038/s41594-020-0439-z (2020).

16 Oz, M., El Nebrisi, E. G., Yang, K. S., Howarth, F. C. & Al Kury, L. T. Cellular and Molecular Targets of Menthol Actions. *Frontiers in pharmacology* **8**, 472, doi:10.3389/fphar.2017.00472 (2017).

17 ECCLES, R. Menthol and Related Cooling Compounds. *Journal of Pharmacy and Pharmacology* **46**, 618-630, doi:10.1111/j.2042-7158.1994.tb03871.x (1994).

18 Karashima, Y. *et al.* Bimodal action of menthol on the transient receptor potential channel TRPA1. *Journal of Neuroscience* **27**, 9874-9884, doi:10.1523/JNEUROSCI.2221-07.2007 (2007).

19 Macpherson, L. J. *et al.* More than cool: Promiscuous relationships of menthol and other sensory compounds. *Molecular and Cellular Neuroscience* **32**, 335-343, doi:10.1016/j.mcn.2006.05.005 (2006).

20 Xu, H., Blair, N. T. & Clapham, D. E. Camphor activates and strongly desensitizes the transient receptor potential vanilloid subtype 1 channel in a vanilloid-independent

mechanism. *Journal of Neuroscience* **25**, 8924-8937, doi:10.1523/JNEUROSCI.2574-05.2005 (2005).
21 Bandell, M. *et al.* High-throughput random mutagenesis screen reveals TRPM8 residues specifically required for activation by menthol. *Nature neuroscience* **9**, 493-500, doi:10.1038/nn1665 (2006).
22 Xiao, B. *et al.* Identification of transmembrane domain 5 as a critical molecular determinant of menthol sensitivity in mammalian TRPA1 channels. *Journal of Neuroscience* **28**, 9640-9651, doi:10.1523/JNEUROSCI.2772-08.2008 (2008).
23 Takaishi, M. *et al.* Reciprocal effects of capsaicin and menthol on thermosensation through regulated activities of TRPV1 and TRPM8. *Journal of Physiological Sciences* **66**, 143-155, doi:10.1007/s12576-015-0427-y (2016).
24 Sánchez, M. E., Turina, A. D. V., García, D. A., Nolan, M. V. & Perillo, M. A. Surface activity of thymol: Implications for an eventual pharmacological activity. *Colloids and Surfaces B: Biointerfaces* **34**, 77-86, doi:10.1016/j.colsurfb.2003.11.007 (2004).
25 Turina, A. d. V., Nolan, M. V., Zygadlo, J. A. & Perillo, M. A. Natural terpenes: Self-assembly and membrane partitioning. *Biophysical Chemistry* **122**, 101-113, doi:10.1016/j.bpc.2006.02.007 (2006).
26 Reiner, G. N., Labuckas, D. O. & García, D. A. Lipophilicity of some GABAergic phenols and related compounds determined by HPLC and partition coefficients in different systems. *Journal of Pharmaceutical and Biomedical Analysis* **49**, 686-691, doi:10.1016/j.jpba.2008.12.040 (2009).
27 Zunino, M. P., Turina, A. V., Zygadlo, J. A. & Perillo, M. A. Stereoselective effects of monoterpenes on the microviscosity and curvature of model membranes assessed by DPH steady-state fluorescence anisotropy and light scattering analysis. *Chirality* **23**, 867-877, doi:10.1002/chir.20998 (2011).
28 Morris, G. M. *et al.* AutoDock4 and AutoDockTools4: Automated docking with selective receptor flexibility. *Journal of computational chemistry* **30**, 2785-2791, doi:10.1002/jcc.21256 (2009).
29 Bayly, C. I., Cieplak, P., Cornell, W. & Kollman, P.A. A Well-Behaved Electrostatic Potential Based Method Using Charge Restraints for Deriving Atomic Charges: The RESP Model. *Journal of Physical Chemistry* **97**, doi:10.1021/j100142a004, (1993).
30 Frisch, M. J. e. a. Gaussian 16. *Revision B.01 (Gaussian, Inc., Wallingford, CT, 2016)*.
31 Wang, J., Wolf, R. M., Caldwell, J. W., Kollman, P. A. & Case, D. A. Development and testing of a general amber force field. *Journal of computational chemistry* **25**, 1157-1174, doi:10.1002/jcc.20035 (2004).
32 Okumura, H. Temperature and pressure denaturation of chignolin: folding and unfolding simulation by multibaric-multithermal molecular dynamics method. *Proteins* **80**, 2397-2416, doi:10.1002/prot.24125 (2012).
33 Okumura, H. & Itoh, S. G. Amyloid fibril disruption by ultrasonic cavitation: nonequilibrium molecular dynamics simulations. *Journal of the American Chemical Society* **136**, 10549-10552, doi:10.1021/ja502749f (2014).
34 Maier, J. A. *et al.* ff14SB: Improving the Accuracy of Protein Side Chain and Backbone Parameters from ff99SB. *Journal of chemical theory and computation* **11**, 3696-3713, doi:10.1021/acs.jctc.5b00255 (2015).
35 Essmann U., P. L., and Berkowitz.L.M A Smooth Particle Mesh Ewald Method. *J. Chem. Phys.* **103**, 8577-8593 (1995).
36 Nosé, S. A molecular dynamics method for simulations in the canonical ensemble. *Molecular Physics* **52**, 255-268, doi:10.1080/00268978400101201 (2006).

37 Hoover, W. G. Canonical dynamics: Equilibrium phase-space distributions. *Physical review. A, General physics* **31**, 1695-1697, doi:10.1103/physreva.31.1695 (1985).
38 Tuckerman, M., Berne, B. J. & Martyna, G. J. Reversible multiple time scale molecular dynamics. *The Journal of Chemical Physics* **97**, 1990-2001, doi:10.1063/1.463137 (1992).
39 Gupta, R. *et al.* Structural basis of TRPA1 inhibition by HC-030031 utilizing species-specific differences. *Scientific reports* **6**, 37460, doi:10.1038/srep37460 (2016).
40 Voets, T., Owsianik, G., Janssens, A., Talavera, K. & Nilius, B. TRPM8 voltage sensor mutants reveal a mechanism for integrating thermal and chemical stimuli. *Nature Chemical Biology* **3**, 174-182, doi:10.1038/nchembio862 (2007).
41 Doerner, J. F., Hatt, H. & Ramsey, I. S. Voltage- and temperature-dependent activation of TRPV3 channels is potentiated by receptor-mediated PI(4,5)P2 hydrolysis. *J Gen Physiol* **137**, 271-288, doi:10.1085/jgp.200910388 (2011).
42 Xiao, R., Tian, J., Tang, J. & Zhu, M. X. The TRPV3 mutation associated with the hairless phenotype in rodents is constitutively active. *Cell Calcium* **43**, 334-343, doi:10.1016/j.ceca.2007.06.004 (2008).
43 Boukalova, S., Teisinger, J. & Vlachova, V. Protons stabilize the closed conformation of gain-of-function mutants of the TRPV1 channel. *Biochimica et Biophysica Acta - Molecular Cell Research* **1833**, 520-528, doi:10.1016/j.bbamcr.2012.11.017 (2013).
44 Boukalova, S., Marsakova, L., Teisinger, J. & Vlachova, V. Conserved residues within the putative S4-S5 region serve distinct functions among thermosensitive vanilloid transient receptor potential (TRPV) channels. *Journal of Biological Chemistry* **285**, 41455-41462, doi:10.1074/jbc.M110.145466 (2010).
45 Smith, G. D. *et al.* TRPV3 is a temperature-sensitive vanilloid receptor-like protein. *Nature* **418**, 186-190, doi:10.1038/nature00894 (2002).
46 Xu, H. *et al.* TRPV3 is a calcium-permeable temperature-sensitive cation channel. *Nature* **418**, 181-186, doi:10.1038/nature00882 (2002).
47 Cordero-Morales, J. F., Gracheva, E. O. & Julius, D. Cytoplasmic ankyrin repeats of transient receptor potential A1 (TRPA1) dictate sensitivity to thermal and chemical stimuli. *Proceedings of the National Academy of Sciences of the United States of America* **108**, E1184-E1191, doi:10.1073/pnas.1114124108 (2011).
48 Yao, J., Liu, B. & Qin, F. Modular thermal sensors in temperature-gated transient receptor potential (TRP) channels. *Proceedings of the National Academy of Sciences of the United States of America* **108**, 11109-11114, doi:10.1073/pnas.1105196108 (2011).
49 Joseph, J., Wang, S., Lee, J., Ro, J. Y. & Chung, M. K. Carboxyl-terminal domain of transient receptor potential vanilloid 1 contains distinct segments differentially involved in capsaicin- And heat-induced desensitization. *Journal of Biological Chemistry* **288**, 35690-35702, doi:10.1074/jbc.M113.513374 (2013).
50 Saito, S. *et al.* Evolution of heat sensors drove shifts in thermosensation between Xenopus species adapted to different thermal niches. *Journal of Biological Chemistry* **291**, 11446-11459, doi:10.1074/jbc.M115.702498 (2016).
51 Vlachová, V. *et al.* Functional role of C-terminal cytoplasmic tail of rat vanilloid receptor 1. *Journal of Neuroscience* **23**, 1340-1350, doi:10.1523/jneurosci.23-04-01340.2003 (2003).
52 Grandl, J. *et al.* Temperature-induced opening of TRPV1 ion channel is stabilized by the pore domain. *Nature neuroscience* **13**, 708-714, doi:10.1038/nn.2552 (2010).
53 Myers, B. R., Bohlen, C. J. & Julius, D. A Yeast Genetic Screen Reveals a Critical Role for the Pore Helix Domain in TRP Channel Gating. *Neuron* **58**, 362-373, doi:10.1016/j.neuron.2008.04.012 (2008).

54 Cui, Y. *et al.* Selective disruption of high sensitivity heat activation but not capsaicin activation of TRPV1 channels by pore turret mutations. *J Gen Physiol* **139**, 273-283, doi:10.1085/jgp.201110724 (2012).
55 Jara-Oseguera, A., Bae, C. & Swartz, K. J. An external sodium ion binding site controls allosteric gating in TRPV1 channels. *eLife* **5**, doi:10.7554/eLife.13356 (2016).
56 Clapham, D. E. & Miller, C. A thermodynamic framework for understanding temperature sensing by transient receptor potential (TRP) channels. *Proceedings of the National Academy of Sciences of the United States of America* **108**, 19492-19497, doi:10.1073/pnas.1117485108 (2011).
57 Hu, H., Rg Grandl, J., Bandell, M., Petrus, M. & Patapoutian, A.
58 Hu, H. Z. *et al.* 2-Aminoethoxydiphenyl borate is a common activator of TRPV1, TRPV2, and TRPV3. *Journal of Biological Chemistry* **279**, 35741-35748, doi:10.1074/jbc.M404164200 (2004).
59 Zubcevic, L. *et al.* Conformational ensemble of the human TRPV3 ion channel. *Nature communications* **9**, doi:10.1038/s41467-018-07117-w (2018).
60 OLMSTED, H. C. KERATODERMIA PALMARIS ET PLANTARIS CONGENITALIS. *American Journal of Diseases of Children* **33**, 757, doi:10.1001/archpedi.1927.04130170055008 (1927).
61 Mevorah, B. *et al.* Olmsted syndrome: Mutilating palmoplantar keratoderma with periorificial keratotic plaques. *Journal of the American Academy of Dermatology* **53**, S266-S272, doi:10.1016/j.jaad.2005.03.036 (2005).
62 Lin, Z. *et al.* Exome Sequencing Reveals Mutations in TRPV3 as a Cause of Olmsted Syndrome. doi:10.1016/j.ajhg.2012.02.006 (2012).
63 Singh, A. K. *et al.* Structural basis of temperature sensation by the TRP channel TRPV3. *Nature Structural and Molecular Biology* **26**, 994-998, doi:10.1038/s41594-019-0318-7 (2019).
64 Zhang, F. *et al.* Heat activation is intrinsic to the pore domain of TRPV1. *Proceedings of the National Academy of Sciences of the United States of America* **115**, E317-E324, doi:10.1073/pnas.1717192115 (2017).
65 Griffin, S., Wyllie, S. G. & Markham, J. Determination of octanol-water partition coefficient for terpenoids using reversed-phase high-performance liquid chromatography. *Journal of Chromatography A* **864**, 221-228, doi:10.1016/S0021-9673(99)01009-2 (1999).
66 Wang, H. & Meng, F. The permeability enhancing mechanism of menthol on skin lipids: a molecular dynamics simulation study. *Journal of molecular modeling* **23**, 279, doi:10.1007/s00894-017-3457-y (2017).
67 Singh, A. K., Saotome, K., McGoldrick, L. L. & Sobolevsky, A. I. Structural bases of TRP channel TRPV6 allosteric modulation by 2-APB. *Nature communications* **9**, 1-11, doi:10.1038/s41467-018-04828-y (2018).

8. Figure Legends

Figure 1. Ribbon diagrams of mouse TRPM8, mouse TRPV3, and rat TRPV1 structures.

(A) Three amino acids (tyrosine, Y; glycine, G; arginine, R) are shown in each ribbon model.

(B) Alignment of S4-S5 linker sequences for mouse TRPM8, mouse TRPV1, rat TRPV1, and mouse TRPV3. Conserved arginine and glycine residues are shown by arrows.

Figure 2. Involvement of mouse TRPM8 residues Y745 (S1) and R842 (S4) in the agonistic effect of menthol.

(**A**) Location of amino acids involved in menthol binding by mouse TRPM8 (mTRPM8).

(B) Structure of *l*-menthol.

(C) Representative current traces for HEK293T cells expressing wild type (WT), mTRPM8-Y745H, or mTRPM8-R842H. Insets indicate current-voltage curves obtained at different time points (1, 2, 3) shown in each trace. Holding potentials were -60mV with ramp-pulses (-100 ~ +100mV, 300ms) applied every 3 sec.

(D) Comparison of current densities at ±60 mV in HEK293T cells expressing WT, Y745H, or R842H mTRPM8 (Current density for WT: 749.4 ± 64.8 pA/pF at +60mV and 449.4 ± 28.6 at -60mV, R842H: 345.5 ± 45.2 pA/pF at +60mV and 42.5 ± 7.6 pA/pF at -60mV, Y745H: 166.4 ± 22.3 pA/pF at +60mV and 10.3 ± 3.0 pA/pF at -60mV). Data represent means ± S.E.M. (n = 5-6). Statistical analysis was performed by two samples *t*-test, $^{*}P$ <0.05, $^{**}P$ <0.01 and $^{***}P$ <0.001.

Figure 3. Comparison of current densities for HEK293T cells expressing mouse TRPV3 WT or Y448H activated by menthol, camphor, or 2-APB.

(A) Location of Y448 (S1), R567, and G573S (S4-S5 linker) in mouse TRPV3 (mTRPV3).

(B – D) Comparison of current densities following treatment of HEK293T cells expressing WT or mTRPV3-Y448H with **(B)** menthol (3 mM) (WT: 80.1 ± 3.2 pA/pF at +60mV and 24.1 ± 4.7 at -60mV, Y448H: 90.7 ± 15.2 pA/pF at +60mV and 35.2 ± 9.0 pA/F at -60mV), **(C)** camphor (10 mM) (WT: 711.3 ± 104.6 pA/pF at +60mV and 599.7 ± 77.8 pA/pF at -60mV and Y448H: 649.7 ± 92.6 pA/pF at +60mV and 580.9 ± 77.3 pA/pF at -60mV), or **(D)** 2-APB (300 μM) (WT: 441.4 ± 61.1 pA/pF at +60mV and 270.8 ± 41.9 pA/pF at -60mV and Y448H: 501.1 ± 91.8 pA/pF at +60mV and 377.9 ± 64.6 pA/pF at -60mV) at ±60mV. Holding potentials were -60mV. Data represent means ± S.E.M. (n = 6-14). Statistical analysis was performed by two samples *t*-test, $^{*}P$ <0.05, $^{**}P$ <0.01 and $^{***}P$ <0.001.

Figure 4. Effect of TRPV3 G573S mutation on the agonistic action of menthol, camphor, and 2-APB.

(A) Representative current traces for HEK293T cells expressing WT or mTRPV3-G573S in response to menthol (3 mM) followed by heat stimulation.

(B) Comparison of menthol-activated current densities in HEK293T cells expressing WT or mTRPV3-G573S at ±60 mV (WT: 86.4 ± 12.7 pA/pF at +60 and 26.2 ± 4.3 pA/pF at -60mV, G573S: 14.0 ± 1.9 pA/pF at +60mV and 6.9 ±1.5 pA/pF at -60mV).

(C) Structure of camphor.

(D) Representative current traces for WT or mTRPV3-G573S in response to camphor (10 mM) followed by heat stimulation.

(E) Comparison of camphor-activated current densities in HEK293T cells expressing WT or mTRPV3-G573S at ±60 mV (WT: 466.0 ± 43.5 pA/pF at +60mV and 410.8 ± 29.6 pA/pF at -60mV, G573S: 18.6 ± 6.7 pA/pF at +60mV and 9.6 ± 3.9 pA/pF).

(F) Structure of 2-APB.

(G) Representative current traces for WT or mTRPV3-G573S in response to 2-APB (300 μM)

followed by heat stimulation.

(H) Comparison of 2-APB-activated current densities in HEK293T cells expressing WT or mTRPV3-G573S at ±60 mV (WT: 310.9 ± 59.7 pA/pF at +60mV and 187.7 ± 25.3 pA/pF at -60mV, G573S: 10.7 ± 1.5 pA/pF at +60mV and 5.1 ± 1.0 pA/pF). Insets in (B), (E), and (H) indicate current-voltage curves obtained at the different time points (1, 2, 3) shown in each trace. Holding potentials were -60mV with ramp-pulses (-100 ~ +100mV, 300ms) applied every 3 sec. Data represent means ± S.E.M. (n = 4-25). Statistical analysis was performed by two samples *t*-test, $^{*}P$ <0.05, $^{**}P$ <0.01 and $^{***}P$ <0.001.

Figure 5. Agonistic effect of menthol, but not camphor, involves R567 in mouse TRPV3.

(A) Representative current traces for HEK293T cells expressing wild type (WT) or R567K mutant stimulated with menthol (3 mM) followed by camphor (10 mM).

(B) Comparison of the normalized current densities ($I_{menthol}/I_{camphor}$) at ±60 mV (WT: 0.16 ± 0.03 at -60mV and 0.08 ± 0.02 at +60mV, R567K: 0.07 ± 0.02 at +60mV and 0.02 ± 0.01 at -60mV).

(C) Comparison of camphor-activated current densities for HEK293T cells expressing WT or mTRPV3-R567K at ±60 mV (WT: 736.5 ± 198.8 pA/pF at +60mV and 633.5 ± 153.6 pA/pF at -60mV, R567K: 634.9 ± 68.2 pA/pF at +60mV and 613.6 ± 35.7 pA/pF at -60mV). Holding potentials were -60mV with ramp-pulses (-100 ~ +100mV, 300ms) every 3 sec. Data represent means ± S.E.M. (n = 6-13). Statistical analysis was performed by two samples *t*-test, $^{*}P$ <0.05, $^{**}P$ <0.01 and $^{***}P$ <0.001.

Figure 6. Response of HEK293T cells expressing WT or R567K of mouse TRPV3 to menthol, camphor, or 2-APB.

(A) Responses to camphor (10 mM, first) and menthol (3 mM, second) by HEK293T cells

expressing WT or mTRPV3-R567K. Holding potentials were -60mV with ramp-pulses (-100 ~ +100mV, 300ms) applied every 3 sec.

(B) Comparison of normalized current densities ($I_{menthol}/I_{camphor}$) in HEK293T cells expressing WT or mTRPV3-R567K at ±60mV (WT: 0.31 ± 0.09 at +60mV and 0.2 ± 0.08 at -60mV, R567K: 0.06 ± 0.01 at +60mV and 0.02 ± 0.003 at +60mV). Data represent means ± S.E.M. (n = 7-9). Statistical analysis was performed by two samples *t*-test, * P <0.05, ** P <0.01 and *** P <0.001.

(C) Dose-dependent curves of 2-APB-activated currents for WT (black) and mTRPV3-R567K (red) at +60 mV (left) and -60 mV (right) (EC_{50} values for WT 113.3 ± 75 μM and 134.4 ± 81 μM at +60 and −60 mV, R567K: 99.4 ± 35 μM and 123.5 ± 33 μM at +60 and −60 mV). For WT, Hill co-efficient values are 2.7 and 2.8 at +60 and -60 mV, respectively, and for mTRPV3-R567K are 2.5 and 2.3 at +60 and -60 mV, respectively. Curves were fit with the data (n = 4-14).

Figure 7. Effect of rat TRPV1 mutations Y441H, **G563S and R557K on the agonistic action of capsaicin and menthol.**

(A) Location of residues Y441 (S1), R557 (bottom of S4), and G563 (S4-S5 linker) in rat TRPV1 (rTRPV1).

(B) Comparison of densities of currents activated by capsaicin (1 μM) in HEK293T cells expressing WT or rTRPV1-Y441H at ±60mV (WT: 706.0 ± 137.0 pA/pF at +60mV and 549.3 ± 75.0 pA/pF at -60mV, Y441H: 125.7 ± 47.1 pA/pF at + 60mV and 26.6 ± 15.4 pA/pF at -60mV). Data represent means ± S.E.M. (n = 5).

(C) Representative current traces for HEK293T cells expressing WT, G563S, or R557K rTRPV1 in response to menthol (3 mM) followed by capsaicin (CAP, 1 μM) stimulation.

(D) Comparison of normalized current densities ($I_{menthol}/I_{CAP}$) for WT, rTRPV1-G563S, or

rTRPV1- R557K expressed by HEK293T cells at ±60mV (WT: 0.08 ± 0.01, G563S: 0.03 ± 0.003, R557K: 0.01 ± 0.002 at +60 mV).

(E) Comparison of CAP-activated currents densities for WT, rTRPV1-G563S, or rTRPV1-R557K expressed in HEK293T cells at ±60mV (WT: 547 ± 26.7 pA/pF at +60 mV and 442 ± 29.2 pA/pF at -60 mV, G563S: 521 ± 3.7 pA/pF at +60 mV and 388.1 ± 26.4 pA/pF at -60 mV; R557K: 633.5 ± 3.31 pA/pF at +60 mV and 476.4 ± 33.8 pA/pF at -60 mV). Holding potentials were -60mV with ramp-pulses (-100 ~ +100mV, 300ms) applied every 3 sec. Data represent means ± S.E.M. (n = 10-22). Statistical analysis was performed using two samples *t*-test, $^{*}P$ <0.05, $^{**}P$ <0.01 and $^{***}P$ <0.001.

Figure 8. Dose-dependent values of capsaicin for activation of WT, G563S or R557K rat TRPV1

Curves (n=4-22) were fit with data for +60 mV (**A**) and +60 mV (**B**) of WT (black), rTRPV1-G563S (red) or rTRPV1-R557K (green) (EC_{50} values for WT: 140 ± 4 nM at +60 mV and 88 ± 30 nM at -60 mV, G563S: 180 ± 30 nM at +60 mV and 154 ± 10 nM at -60 mV, R557K: 156 ± 30 nM at +60 mV and 124 ± 30 nM at -60 mV). For WT, the Hill co-efficient values are 2.4 and 2.4 at +60 and -60 mV, respectively, for rTRPV1-G563S are 2.0 and 2.0 at +60 and -60 mV, respectively, and for rTRPV1-R557K are 1.8 and 2.0 at +60 and -60 mV, respectively. Statistical analysis was performed by two samples *t*-test, $^{*}P$ <0.05, $^{**}P$ <0.01 and $^{***}P$ <0.001.

Figure 9. Effect of rat TRPV1 mutations G563S and R557K on agonistic action of camphor and 2-APB.

(A) Representative current traces for HEK293T cells expressing WT, rTRPV1-G563S, or rTRPV1-R557K stimulated with camphor (10 mM) followed by CAP (1 μM).

(B) Representative current traces for HEK293T cells expressing WT, rTRPV1-G563S, or

rTRPV1-R557K stimulated with 2-APB (300 μM) followed by CAP (1 μM).

(C) Comparison of the normalized current densities ($I_{camphor}/I_{CAP}$) for WT, rTRPV1-G563S, or rTRPV1-R557K expressed in HEK293T cells at ±60mV ($I_{camphor}/I_{CAP}$ for WT: 0.63 ± 0.07 at +60 mV and 0.28 ± 0.06 at -60 mV, G563S: 0.03 ± 0.01 at +60 mV and 0.02 ± 0.01 at -60 mV, R557K: 0.03 ± 0.01 at +60 mV and 0.02 ± 0.01 at -60 mV).

(D) Comparison of normalized current densities ($I_{2\text{-}APB}/I_{CAP}$) in HEK293T cells expressing WT, rTRPV1-G563S, or rTRPV1-R557K at ±60mV (WT: 0.84 ± 0.06 at +60 mV and 0.91 ± 0.08 at -60 mV, G563S: 0.03 ± 0.004 at +60 mV and 0.02 ± 0.004 at -60 mV, R557K: 0.02 ± 0.001 at +60 mV and 0.02 ± 0.002 at -60mV). Holding potentials were -60mV with ramp-pulses (-100 ~ +100mV, 300ms) applied every 3 sec. Data represent means ± S.E.M. (n = 8-15). Statistical analysis was performed using two samples *t*-test, $^{*}P$ <0.05, $^{**}P$ <0.01 and $^{***}P$ <0.001.

Figure 10. Responses of WT, R567H, R567K, or R567F mouse TRPV3 to 2-APB, camphor, or menthol and positive charge of R567 is essential for camphor-evoked activation of mouse TRPV3.

(A) Representative traces of currents elicited in response to 2-APB (300 μM, first) and camphor (10 mM, second) in HEK293T cells expressing WT, mTRPV3-R567H, mTRPV3-R567K, mTRPV3-R567A or mTRPV3-R567F. Holding potentials were -60mV with ramp-pulses (-100 ~ +100mV, 300ms) applied every 3 sec.

(B) Comparison of normalized current densities ($I_{camphor}/I_{2\text{-}APB}$) in HEK293T cells expressing WT, mTRPV3-R567K, mTRPV3-R567H, mTRPV3-R567A, or mTRPV3-R567F at ±60mV ($I_{camphor}/I_{2\text{-}APB}$ of R567A: 0.21 ± 0.02 at +60 mV and 0.25 ± 0.03 at -60 mV, R567F: 0.13 ± 0.01 at -60 mV and 0.18 ± 0.03 at -60 mV) compared with WT, R567K and R567H (WT: 1.93 ± 0.25 at +60 mV and 2.79 ± 0.48 at -60 mV, R567K: 1.81 ± 0.22 at +60 mV and 1.95 ± 0.34

at -60 mV, R567H: 1.77 ± 0.17 at +60 mV and 1.92 ± 0.28 at -60 mV). Holding potentials were -60mV with ramp-pulses (-100 ~ +100mV, 300ms) applied every 3 sec. Data represent means ± S.E.M. (n = 9-16). Statistical analysis was performed by one-way ANOVA, $^{*}P$ <0.05 (R567A vs. R567K, R567H at -60 mV), $^{**}P$ <0.01 (R567F vs. R567K, R567H at -60 mV) and $^{***}P$ <0.001 (R567A vs. WT, R567K, R567H at +60 mV; R567F vs. WT, R567K, R567H at +60 mV; R567A vs. WT at -60 mV; R567F vs. WT at -60 mV).

(C) Representative traces of currents elicited in response to 2-APB (300 μM, first) and menthol (3 mM, second) in HEK293T cells expressing WT or mTRPV3-R567F. Holding potentials were -60mV with ramp-pulses (-100 ~ +100mV, 300ms) applied every 3 sec.

Figure 11. Heat-evoked currents for WT and mutated mouse TRPV3 and rat TRPV1.

(A) Representative current (upper) and temperature (lower) traces for HEK293T cells expressing WT, mTRPV3-G573S, or mTRPV3-R567K exposed to heat up to 53 ˚C.

(B) Representative Arrhenius plots from currents activated by heat stimulation of HEK293T cells expressing WT, mTRPV3-G573S or mTRPV3-R567K at -60 mV. Gray dotted lines indicate linear fits of the plots before and after heat-evoked activation, and red dotted lines indicate temperature thresholds at the intersection of the gray dotted lines.

(C) Comparison of heat-evoked current densities (left) and temperature thresholds (right) in HEK293T cells expressing WT, mTRPV3-G573S, or mTRPV3-R567K at -60mV (WT: 211.3 ± 38.1 pA/pF, G573S: 233.1 ± 63.9 pA/pF, R567K: 262.7 ± 54.4 pA/pF).

(D) Representative current (upper) and temperature (lower) traces for HEK293T cells expressing WT, rTRPV1-G563S, or rTRPV1-R557K exposed to heat up to 45 ˚C (WT: 50.2 ± 0.6 °C, G573S: 50.2 ± 1.5 °C, R567K: 51.3 ± 0.4 °C).

(E) Comparison of heat-evoked current densities for HEK293T cells expressing WT, rTRPV1-G563S, or rTRPV1-R557K at -60mV (WT: 40.8 ± 10.1 pA/pF, G563S: 6.5 ± 0.6 pA/pF,

R557K: 4.5 ± 0.6 pA/pF). Holding potentials were -60mV. Data represent means ± S.E.M. (n = 5-14). Statistical analysis was performed by one-way ANOVA, $^{*}P$ <0.05, $^{**}P$ <0.01 and $^{***}P$ <0.001.

Figure 12. Molecular dynamics simulation confirming a stable bond between monoterpenes and R567.

Typical snapshots of (**A**) menthol in WT TRPV3, (**B**) camphor in WT TRPV3, (**C**) menthol in mTRPV3-R567F, (**D**) camphor in mTRPV3-R567F. Pink highlight means the hydrogen bonds between monoterpenes and R567. Time series of distance between (**E**) menthol and R567/F567 and (**F**) camphor and R567/F567.

Figure 1

A

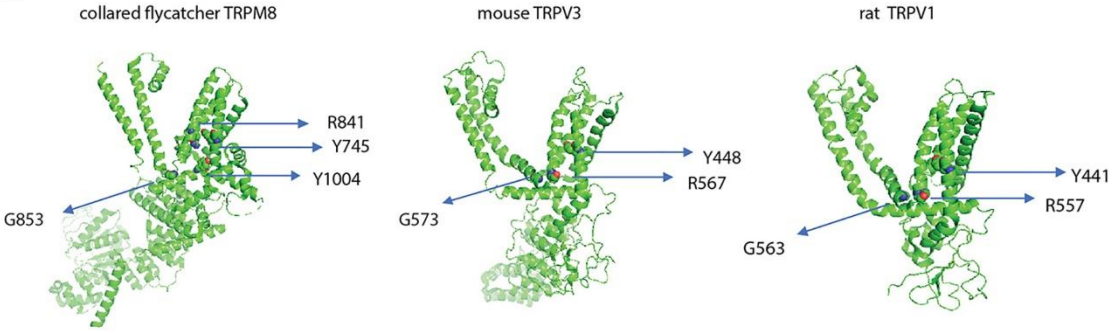
collared flycatcher TRPM8
mouse TRPV3
rat TRPV1
R841
Y745
Y1004
G853
Y448
R567
G573
Y441
R557
G563

B

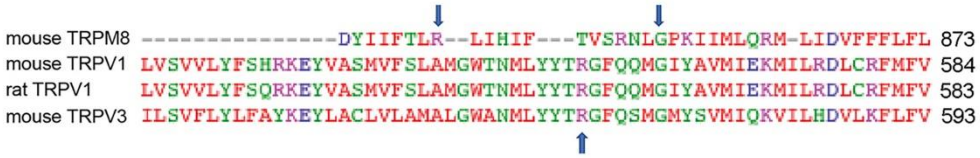
mouse TRPM8 ----------DYIIFTLR--LIHIF---TVSRNLGPKIIMLQRM-LIDVFFFLFL 873
mouse TRPV1 LVSVVLYFSHRKEYVASMVFSLAMGWTNMLYYTRGFQQMGIYAVMIEKMILRDLCRFMFV 584
rat TRPV1 LVSVVLYFSQRKEYVASMVFSLAMGWTNMLYYTRGFQQMGIYAVMIEKMILRDLCRFMFV 583
mouse TRPV3 ILSVFLYLFAYKEYLACLVLAMALGWANMLYYTRGFQSMGMYSVMIQKVILHDVLKFLFV 593

Figure 2

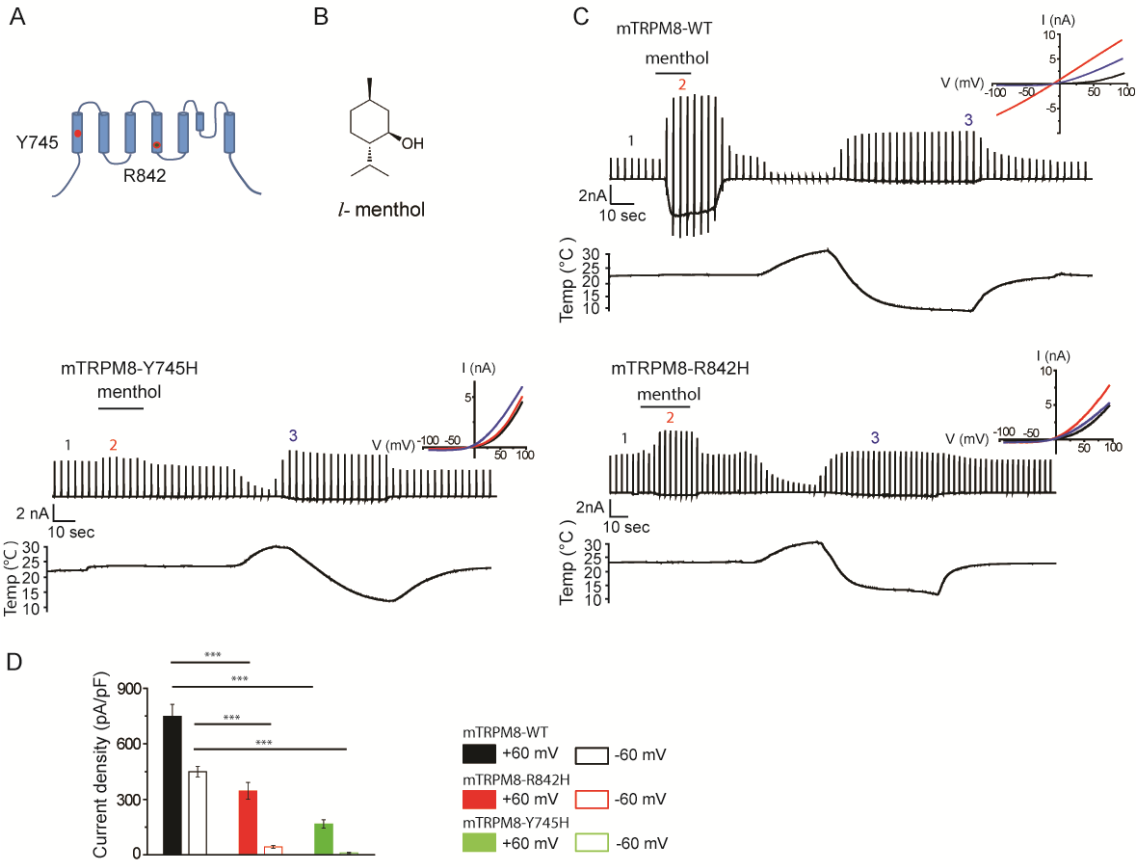
A
Y745
R842
B
OH
l- menthol
C
mTRPM8-WT
menthol
I (nA)
V (mV)
2nA
10 sec
Temp (°C)
mTRPM8-Y745H
menthol
2 nA
10 sec
mTRPM8-R842H
menthol
D
Current density (pA/pF)
***
mTRPM8-WT
+60 mV
-60 mV
mTRPM8-R842H
+60 mV
-60 mV
mTRPM8-Y745H
+60 mV
-60 mV

Figure 3

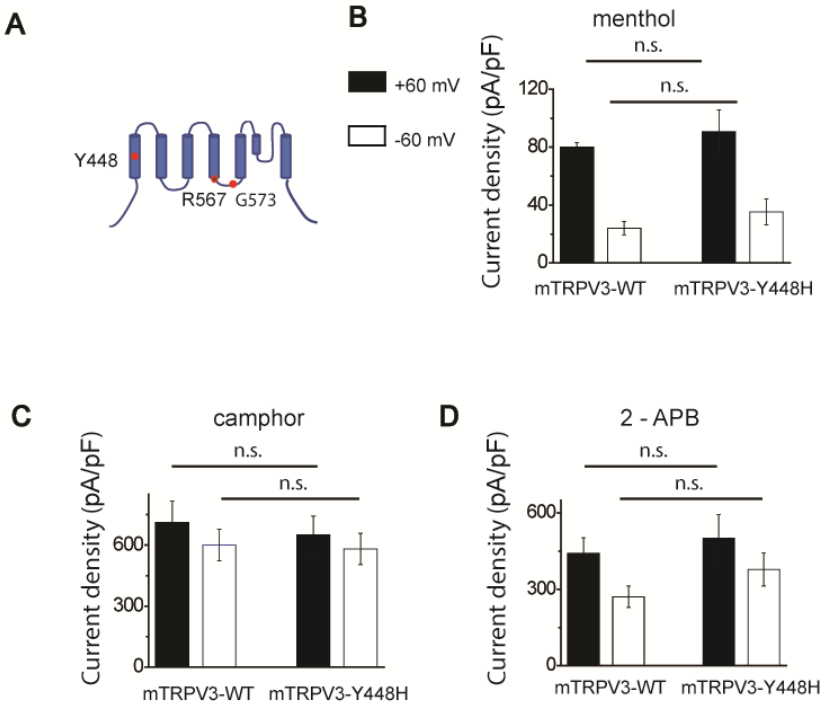
A
Y448
R567
G573
B
+60 mV
-60 mV
menthol
n.s.
n.s.
Current density (pA/pF)
120
80
40
0
mTRPV3-WT
mTRPV3-Y448H
C
camphor
n.s.
n.s.
Current density (pA/pF)
600
300
0
mTRPV3-WT
mTRPV3-Y448H
D
2 - APB
n.s.
n.s.
Current density (pA/pF)
600
300
0
mTRPV3-WT
mTRPV3-Y448H

Figure 4

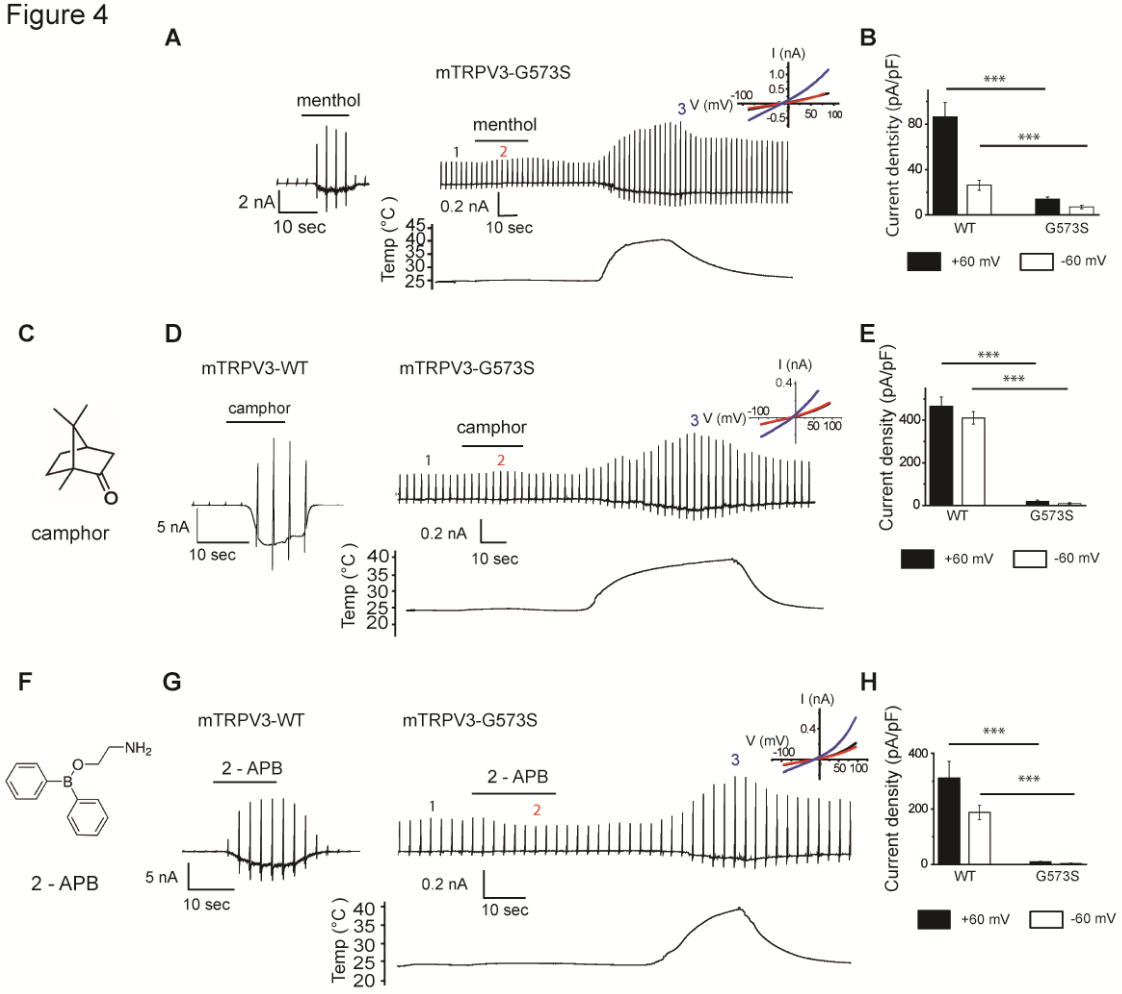
A
menthol
2 nA
10 sec
mTRPV3-G573S
menthol
1
2
3
V (mV)
I (nA)
0.2 nA
10 sec
Temp (°C)
B
Current dentsity (pA/pF)
***
***
WT
G573S
+60 mV
-60 mV
C
camphor
D
mTRPV3-WT
mTRPV3-G573S
camphor
5 nA
10 sec
0.2 nA
10 sec
Temp (°C)
E
Current density (pA/pF)
WT
G573S
+60 mV
-60 mV
F
2 - APB
G
mTRPV3-WT
mTRPV3-G573S
2 - APB
5 nA
10 sec
0.2 nA
10 sec
Temp (°C)
H
Current density (pA/pF)
WT
G573S
+60 mV
-60 mV

Figure 5

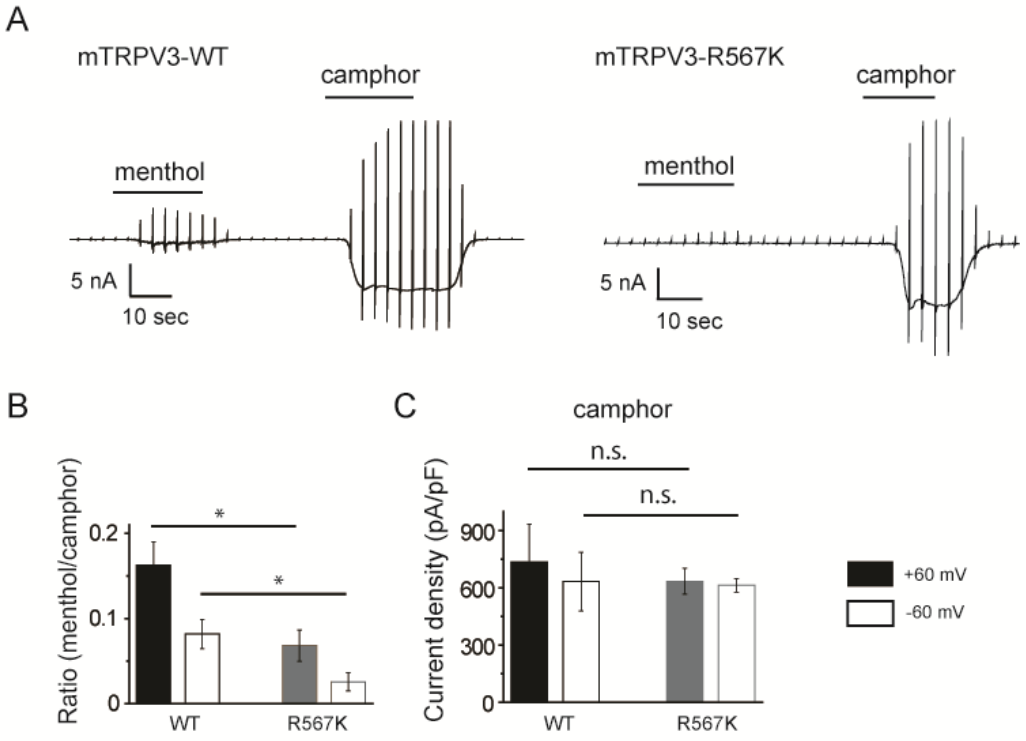
A
mTRPV3-WT
camphor
menthol
5 nA
10 sec
mTRPV3-R567K
camphor
menthol
5 nA
10 sec
B
Ratio (menthol/camphor)
0.2
0.1
0
*
*
WT
R567K
C
camphor
n.s.
n.s.
Current density (pA/pF)
900
600
300
0
WT
R567K
+60 mV
-60 mV

Figure 6

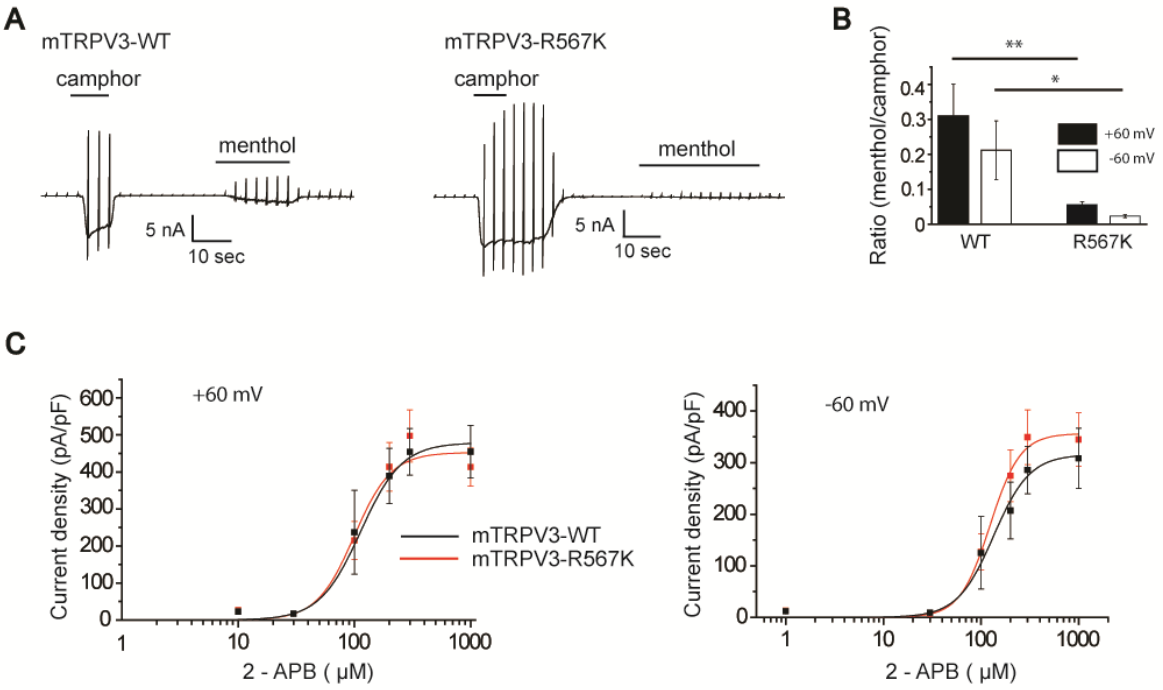
A
mTRPV3-WT
camphor
menthol
5 nA
10 sec
mTRPV3-R567K
camphor
menthol
5 nA
10 sec
B
Ratio (menthol/camphor)
**
*
+60 mV
-60 mV
WT
R567K
C
+60 mV
Current density (pA/pF)
mTRPV3-WT
mTRPV3-R567K
2 - APB (μM)
-60 mV
Current density (pA/pF)
2 - APB (μM)

Figure 7

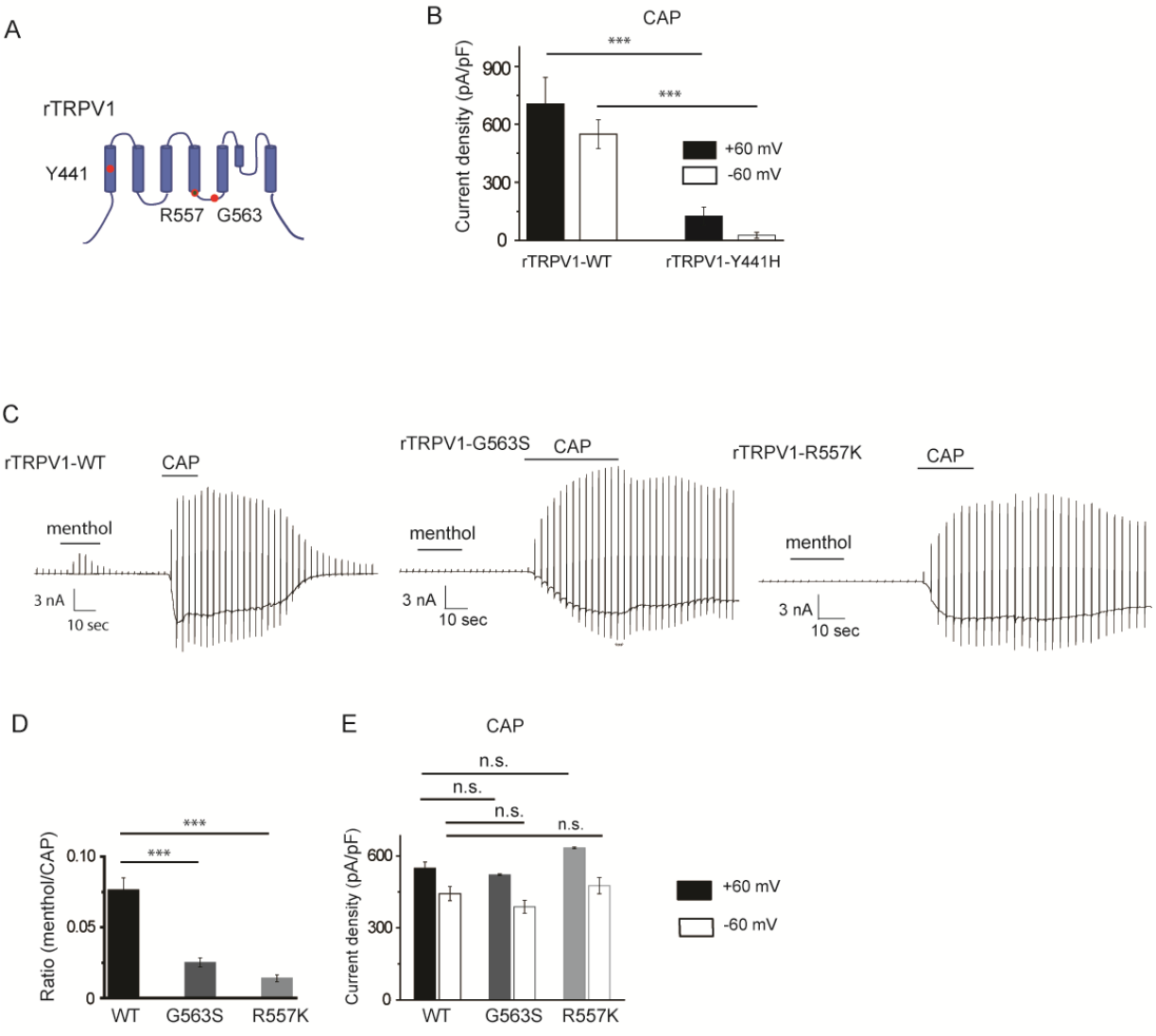
A
rTRPV1
Y441
R557
G563
B
CAP
***
***
Current density (pA/pF)
900
600
300
0
+60 mV
-60 mV
rTRPV1-WT
rTRPV1-Y441H
C
rTRPV1-WT
CAP
menthol
3 nA
10 sec
rTRPV1-G563S
CAP
menthol
3 nA
10 sec
rTRPV1-R557K
CAP
menthol
3 nA
10 sec
D
***
***
Ratio (menthol/CAP)
0.10
0.05
0
WT
G563S
R557K
E
CAP
n.s.
n.s.
n.s.
n.s.
Current density (pA/pF)
600
300
0
WT
G563S
R557K
+60 mV
-60 mV

Figure 8

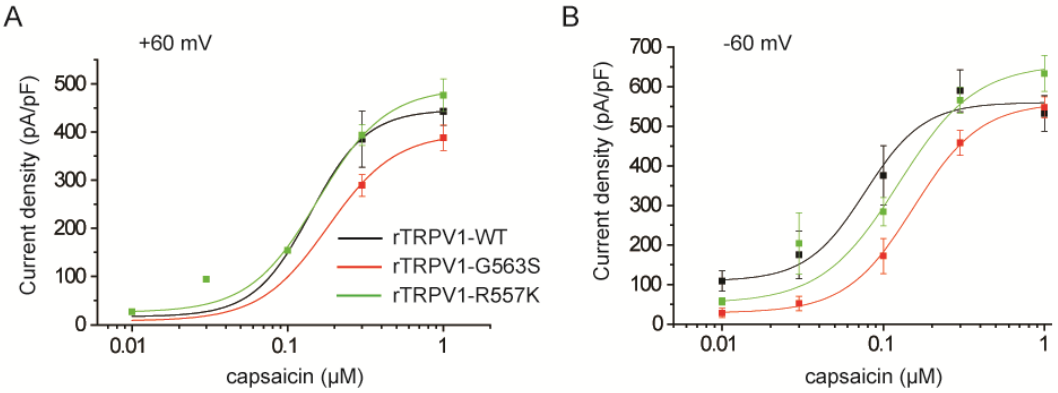
A
+60 mV
Current density (pA/pF)
0
100
200
300
400
500
0.01
0.1
1
capsaicin (μM)
rTRPV1-WT
rTRPV1-G563S
rTRPV1-R557K
B
-60 mV
Current density (pA/pF)
0
100
200
300
400
500
600
700
0.01
0.1
1
capsaicin (μM)

Figure 9

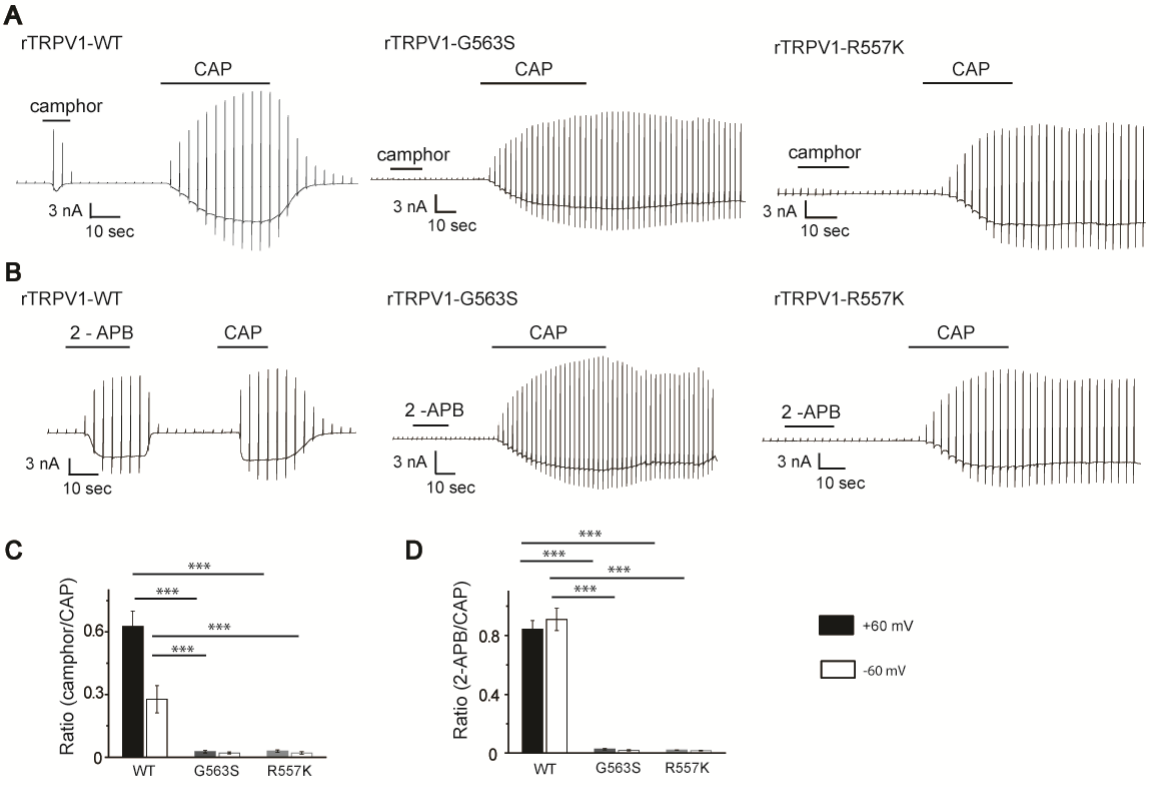
A
rTRPV1-WT
CAP
camphor
3 nA
10 sec
rTRPV1-G563S
CAP
camphor
3 nA
10 sec
rTRPV1-R557K
CAP
camphor
3 nA
10 sec
B
rTRPV1-WT
2 - APB
CAP
3 nA
10 sec
rTRPV1-G563S
CAP
2 -APB
3 nA
10 sec
rTRPV1-R557K
CAP
2 -APB
3 nA
10 sec
C
Ratio (camphor/CAP)
0
0.3
0.6
***
***
***
***
WT
G563S
R557K
D
Ratio (2-APB/CAP)
0
0.4
0.8
***
***
***
***
WT
G563S
R557K
+60 mV
-60 mV

Figure 10

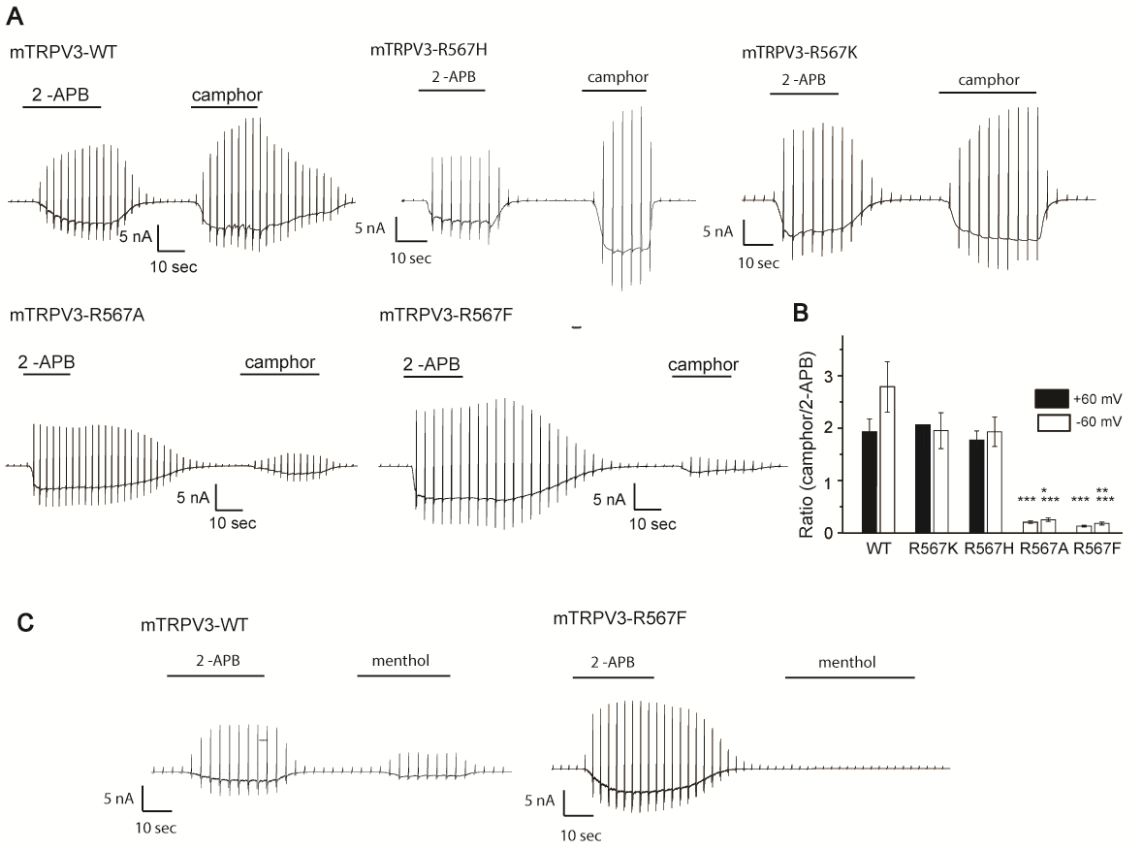
A
mTRPV3-WT
2 -APB
camphor
5 nA
10 sec
mTRPV3-R567H
2 -APB
camphor
5 nA
10 sec
mTRPV3-R567K
2 -APB
camphor
5 nA
10 sec
mTRPV3-R567A
2 -APB
camphor
5 nA
10 sec
mTRPV3-R567F
2 -APB
camphor
5 nA
10 sec
B
Ratio (camphor/2-APB)
0
1
2
3
+60 mV
-60 mV
WT
R567K
R567H
R567A
R567F

C
mTRPV3-WT
2 -APB
menthol
5 nA
10 sec
mTRPV3-R567F
2 -APB
menthol
5 nA
10 sec

Figure 11

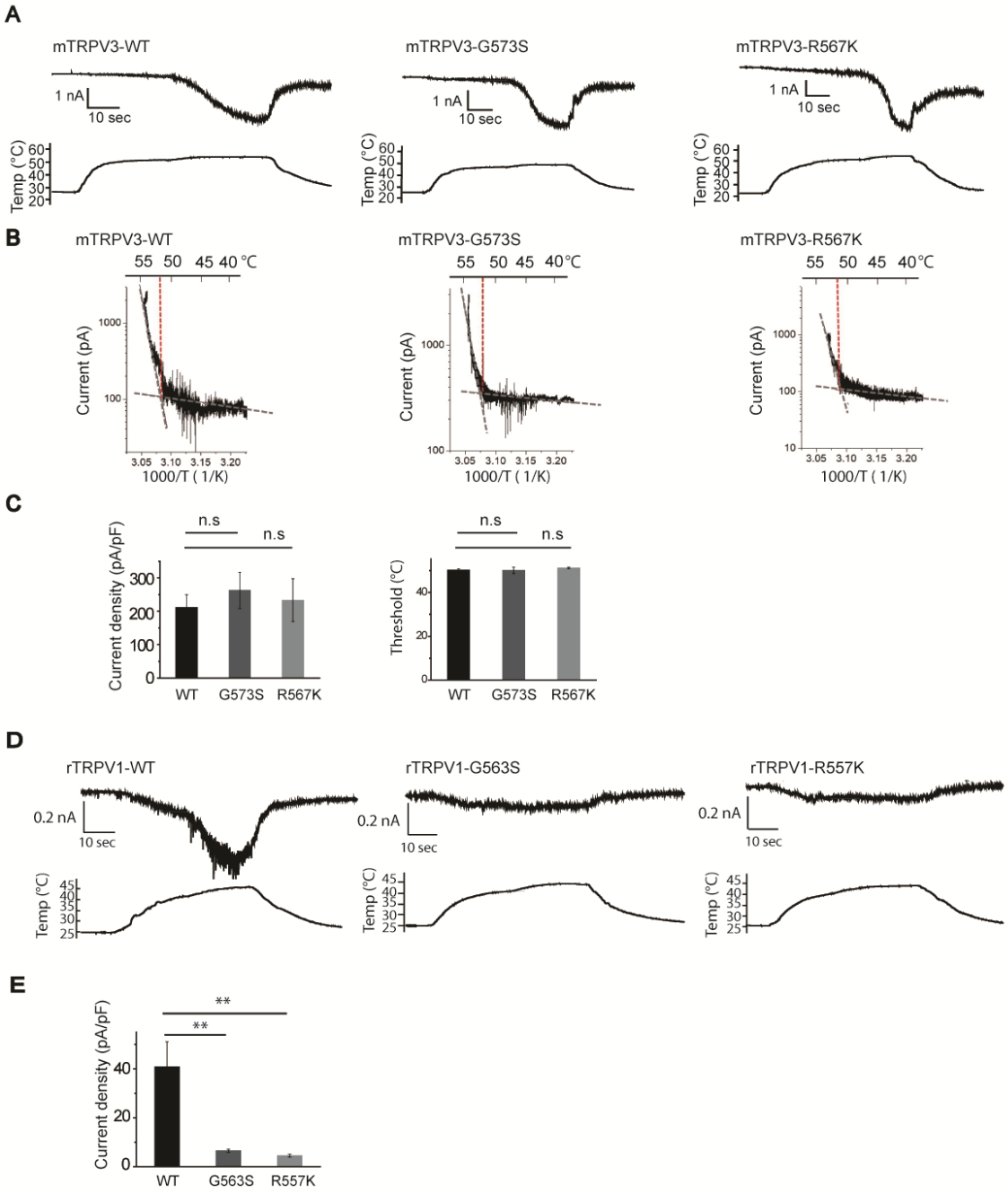
A
mTRPV3-WT
mTRPV3-G573S
mTRPV3-R567K
1 nA
10 sec
Temp (°C)
B
mTRPV3-WT
mTRPV3-G573S
mTRPV3-R567K
55 50 45 40 °C
Current (pA)
1000/T (1/K)
C
n.s
Current density (pA/pF)
Threshold (°C)
WT
G573S
R567K
D
rTRPV1-WT
rTRPV1-G563S
rTRPV1-R557K
0.2 nA
10 sec
Temp (°C)
E
**
Current density (pA/pF)
WT
G563S
R557K

Figure 12

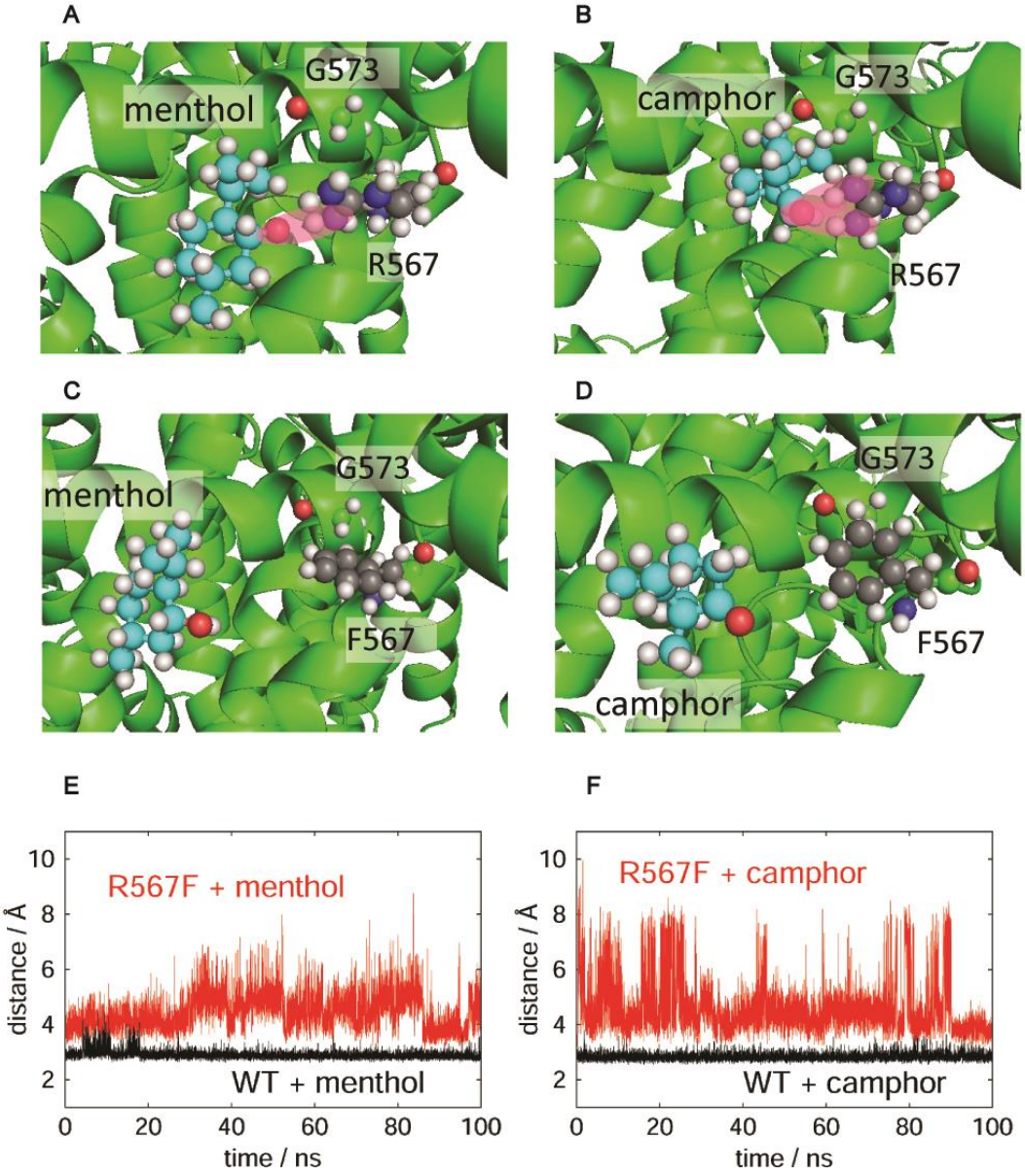
A
menthol
G573
R567
B
camphor
G573
R567
C
menthol
G573
F567
D
G573
F567
camphor
E
R567F + menthol
WT + menthol
distance / Å
time / ns
F
R567F + camphor
WT + camphor
distance / Å
time / ns